Methane Flux Gradient Reflects Compositional Shifts in Methane-Cycling Genera Under a Uniform Temperate Peatland Vegetation

Joel D. White

joel.white.2@bioenv.gu.se

University of Gothenburg

Dag Ahrén

University of Gothenburg

Frans-Jan W. Parmentier

University of Oslo

Veiko Lehsten

Mid Sweden University

Janne Rinne

Natural Resources Institute Finland (LUKE)

Lena Ström

Lund University

Article

Keywords:

Posted Date: May 21st, 2026

DOI: https://doi.org/10.21203/rs.3.rs-9440120/v1

Additional Declarations: No competing interests reported.

Abstract

Wetlands are globally significant sources of methane (CH_4). Fine-scale variability in emissions often occurs within visually uniform vegetation communities, suggesting that belowground microbial processes may contribute to otherwise unexplained spatial heterogeneity. Here, we used a captured metagenomics approach targeting taxa associated with CH_4 metabolism pathway (KEGG ko:00680) to examine microbial community composition across nine-mesocosms in a peatland system dominated by *Eriophorum vaginatum*. Despite similar environmental conditions and vegetation composition, CH_4 fluxes varied 2.4-fold among mesocosms and coincided with parallel increases in ecosystem respiration, but not gross primary productivity.

Across the CH_4-cycling community, methanotrophs comprised 55.4% of relative abundance and methanogens 44.6%, indicating substantial representation of both CH_4 oxidation and production potential. Community composition was dominated by a small number of taxa, including the Type II methanotroph *Methylocella*, the hydrogenotrophic methanogen *Methanoregula* and the Type II methanotroph *Methylosinus*. With increasing CH_4 flux, methanogenic communities shifted toward greater representation of acetoclastic and metabolically versatile taxa such as *Methanosarcina* and Methanosaeta, whereas the dominant hydrogenotrophic genus *Methanoregula* declined modestly.

Indicator species analysis identified a diverse suite of methanogenic taxa associated with low emission mesocosms, including *Methanothermococcus*, *Methanohalobium*, *Methanohalophilus*, and *Methanosaeta*. In contrast, methanotrophic indicators occurred at intermediate positions along the CH_4 flux gradient, with *Methylococcus* associated with CH_4 emission order 3 and *Methylosinus* with CH_4 emission order 4. Although methanotrophs were abundant overall, shifts in methanotrophic taxa did not scale proportionally with increasing CH_4 emissions, suggesting that oxidation in these saturated soils may be constrained primarily by oxygen availability rather than CH_4 supply.

These results demonstrate that, even within a single plant functional type, spatial heterogeneity in CH_4 flux reflects fine-scale restructuring of CH_4-cycling microbial communities. Incorporating microbial functional diversity into CH_4 models may improve predictions of peatland carbon climate feedbacks under changing environmental conditions.

Introduction

Methane (CH_4) is a well-mixed greenhouse gas in the atmosphere, with a global warming potential more than 27 times that of carbon dioxide (CO_2) over a 100-year period [1–3]. Atmospheric CH_4 concentrations have more than doubled since pre-industrial times, and, following a period of relative stability, global CH_4 levels are again rising at a rate of approximately 5 ppb per year [2, 3]. Total CH_4 emissions are estimated to contribute ~30% of the increased radiative forcing observed to date [3]. Among natural sources, wetlands are the largest emitters, contributing an estimated 175 Tg CH_4 yr^{-1} (151–229) [3].

CH_4 production in wetlands is driven by methanogenic Archaea, where organic matter is degraded stepwise via hydrolysis and fermentation before being converted into CH_4 through methanogenesis [4, 5]. This process is tightly coupled to methanotrophy, that is, the microbial oxidation of CH_4 by specialized methane-oxidizing bacteria (MOB), including members of the Proteobacteria, Verrucomicrobia, and NC10, which can consume 10–90% of CH_4 before it escapes to the atmosphere [6, 7].

While CH_4 emissions from wetlands are often studied in relation to broad-scale environmental controls, including soil moisture, plant community composition, soil temperature, and substrate availability [8–11], substantial spatial variability in CH_4 fluxes is frequently observed within a single plant community, with few drivers explaining the magnitude of that variation [12, 13]. This spatial heterogeneity presents a challenge for CH_4 modelling, because many models treat microbial processes as static or homogeneous across space and therefore fail to account for variability in microbial community composition or function [14, 15].

Many Earth system and process-based CH_4 models simplify microbial processes into functional approximations or proxies tied to vegetation type or moisture, assuming limited spatial variation in microbial functional composition or activity. However, growing evidence suggests that belowground microbial communities exhibit functional heterogeneity that may be crucial for explaining spatial variability in CH_4 fluxes within otherwise uniform vegetation [14, 16].

Recent advances in molecular biology have enabled more nuanced exploration of microbial community function using marker-gene analysis (for example, mcrA and pmoA) and, increasingly, shotgun metagenomics [17, 18]. Yet traditional metagenomic approaches remain resource-intensive, limiting their application across spatially replicated samples. In response, captured metagenomics has emerged as a targeted, cost-effective strategy for assessing the functional gene repertoire of soil microbial communities by focusing on specific metabolic pathways such as methanogenesis and methanotrophy [19–21]. This approach enables deeper, more focused sequencing of functionally relevant genes without the computational and financial burden of full metagenomes.

Here, we used captured metagenomics to investigate the composition of CH_4-cycling microbial communities in peat-plant mesocosms all dominated by *Eriophorum vaginatum*, a sedge species common in northern peatlands. Specifically, we asked whether (i) the composition of CH_4-producing and CH_4-consuming taxa shifts within a single ecotype dominated by the same plant species, and (ii) specific taxa act as indicators of lower- and higher-emitting CH_4 locations. By addressing these questions, we evaluate whether variation in microbial community structure, even under uniform vegetation type, helps explain persistent spatial variability of CH_4 fluxes in northern peatlands.

Results

Carbon fluxes along the CH_4 gradient

CH_4 and CO_2 fluxes were measured across 9 mesocosms where light levels, temperature and water table depth were kept as similar as possible. All were dominated by the sedge *Eriophorum vaginatum* (see methods for details). CH_4 emissions increased steadily across CH_4 emission orders 1–8, rising from 42.1 ± 15.1 SD nmol CH_4 m^{-2} s^{-1} at emission order 1 to 66.8 ± 3.19 SD nmol CH_4 m^{-2} s^{-1} at emission order 8 (Fig. 1A). Emission order number 9 was distinctly higher than emission orders 1–8, with a mean flux of 103.0 ± 6.56 SD nmol CH_4 m^{-2} s^{-1} (Table 1). Overall, the highest-emitting mesocosm emitted 2.4-fold more CH_4 than the lowest-emitting mesocosm. Linear mixed-effects models confirmed a strong effect of CH_4 emission order on CH_4 (χ^2 = 94.38, df = 8), R_{eco} (χ^2 = 104.61, df = 8), GPP (χ^2 = 73.94, df = 8), and NEE (χ^2 = 42.33, df = 8); all likelihood-ratio tests were significant at $p \leq 0.001$.

Table 1
Summary statistics of methane (CH_4) flux measurements across mesocosms ordered by CH_4 emission order (1–9, lowest to highest mean flux). Values represent mean, standard deviation (SD), median, interquartile range (IQR), minimum (Min), and maximum (Max) across repeated measurements (n = 6 per mesocosm). Original mesocosm number indicated the original numbering patter before percentile ranking

CH_4 Emission Order	**(n)**	**Mean CH_4 (nmol CH_4 m^{-2} s^{-1})**	**SD**	**Median**	**IQR**	**Min**	**Max**	**Original Mesocosm #**
1	6	42.1	15.1	37.0	5.90	33.1	72.4	9
2	6	45.6	3.31	44.8	5.04	41.6	49.6	6
3	6	51.8	2.43	51.3	0.78	49.0	56.3	5
4	6	53.3	9.50	53.5	7.94	36.4	62.3	7
5	6	57.2	5.48	58.3	7.16	50.3	64.6	3
6	6	65.7	4.73	65.1	2.65	61.2	74.7	8
7	6	66.2	4.46	66.3	5.53	60.5	72.7	2
8	6	66.8	3.19	66.4	5.42	63.6	70.8	1
9	6	103.0	6.56	102.0	4.64	94.4	114.0	4

When plotted against mesocosm CH_4 flux, NEE showed no significant relationship, GPP showed a weak but significant relationship, and R_{eco} showed a strong positive relationship. Summary statistics (Supplementary Table 2) showed an approximate doubling of R_{eco} across the CH_4 flux gradient, from 2.35 ± 0.22 SD to 4.36 ± 0.33 SD µmol CO_2 m^{-2} s^{-1}, with emission order 9 exhibiting the highest CH_4 and R_{eco} fluxes, suggesting coordinated shifts in ecosystem carbon cycling (Fig. 1). CH_4 flux was positively related to R_{eco}, explaining a substantial proportion of the variation in emissions (R^2 = 0.34, $p \leq 0.0001$; Fig. 1B).

In contrast, NEE showed no significant relationship with CH_4 flux (adjusted $R^2 = -0.02$; Fig. 1C), despite mean uptake shifting from − 2.55 ± 0.42 SD to − 3.06 ± 0.57 SD μmol CO_2 m^{-2} h^{-1} across the gradient. Although emission order 9 clearly had the highest CH_4 and R_{eco} fluxes, this pattern was not mirrored in GPP. GPP exhibited a weak but significant negative relationship with CH_4 flux (adjusted $R^2 = 0.08$, $p \leq 0.05$; Fig. 1D), indicating that more negative GPP values, and thus greater CO_2 uptake, were weakly associated with CH_4 flux.

Figure 1: CH_4 fluxes across all emission orders (1–9) (A), and linear regressions between CH_4 flux and (B) ecosystem respiration (R_{eco}), (C) net ecosystem exchange (NEE), and (D) gross primary productivity (GPP). Points represent individual flux measurements (n = 54). Solid lines represent fitted polynomial regressions and shaded areas indicate ± 95% confidence intervals. Adjusted R^2 and p-values from linear models are shown in panels B–D.

Relationships between tiller density and carbon fluxes

Across mesocosms, tiller density showed clear relationships with CO_2 fluxes but not with CH_4 (Fig. 2). A linear mixed-effects model with CH_4 emission order as a random intercept indicated that CH_4 flux was not significantly related to tiller density ($R^2 = 0.15$, $p = 0.14$). Thus, mesocosms with denser graminoid cover did not necessarily emit more CH_4.

In contrast, GPP was significantly associated with tiller density ($R^2 = 0.67$, $p \leq 0.001$), with greater tiller numbers linked to more negative GPP values, consistent with increased CO_2 uptake. R_{eco} also scaled positively with tiller density ($R^2 = 0.74$, $p \leq 0.001$), indicating greater CO_2 emission in mesocosms with more aboveground biomass. Finally, NEE was negative overall, and tiller density significantly enhanced net CO_2 uptake ($R^2 = 0.20$, $p \leq 0.05$).

Figure 2

Carbon fluxes of (A) methane (CH_4), (B) ecosystem respiration (Reco), (C) net ecosystem exchange (NEE), and (D) gross primary productivity (GPP) plotted against mean tiller density per mesocosm. Points represent individual mesocosms coloured by CH_4 emission order. Fitted lines and shaded ribbons show model predictions and 95% confidence intervals derived from linear mixed-effects models. Reported statistics indicate marginal R^2 and p-values for the effect of tiller density on each flux.

Microbial community composition

Across the CH_4-cycling community, methanotrophs comprised a slightly greater proportion than methanogens, contributing on average 55.4% and 44.6% of relative abundance, respectively. Community composition was dominated by a small number of genera. The most abundant taxon overall was the Type II methanotroph *Methylocella* (23.6%), followed by the hydrogenotrophic methanogen *Methanoregula* (18.4%) and the Type II methanotroph *Methylosinus* (16.9%). Other abundant taxa

included the metabolically versatile methanogen *Methanosarcina* (9.1%), the Type I methanotroph *Methylococcus* (8.8%), and the *Verrucomicrobial* methanotroph *Methylacidiphilum* (6.1%). Together, these results indicate that both methanogenic and methanotrophic taxa contributed substantially to the curated CH_4-cycling assemblage, with Type II methanotrophs accounting for a particularly large share of the detected community.

Functional restructuring across the CH_4 gradient

The CH_4-cycling community exhibited structured compositional shifts across the CH_4 flux gradient (Fig. 3). Among methanogens, the dominant hydrogenotrophic genus *Methanoregula* remained abundant across all emission orders but declined modestly from emission order 1 to emission order 9 (− 5.3%). In contrast, the acetoclastic and mixotrophic methanogen *Methanosarcina* increased across the gradient (+ 14.0%), and *Methanosaeta* showed a smaller increase (+ 12.4%). Several methylotrophic methanogens, including *Methanohalobium* (+ 11.6%) and *Methanohalophilus* (+ 6.1%), also increased slightly from low- to high-emission mesocosms.

Among methanotrophs, Type II taxa dominated the curated methanotrophic assemblage. *Methylocella* remained the most abundant methanotroph across the gradient and changed little overall (+ 2.2%), whereas *Methylosinus* increased modestly from emission order 1 to emission order 9 (+ 8.2%). In contrast, the *Verrucomicrobial* methanotroph *Methylacidiphilum* declined across the full gradient (− 28.5%), indicating lower representation in higher-emitting mesocosms.

Significant stepwise shifts between adjacent CH_4 emission orders were identified using pairwise t-tests on within-group relative abundance with Benjamini–Hochberg correction. Within methanogens, significant increases between emission orders 1 and 2 were detected for *Methanocella*, *Methanoculleus*, *Methanopyrus*, *Methanothermococcus*, *Methanosaeta*, *Methanohalophilus*, and *Methanohalobium*. Within methanotrophs, *Methylococcus* declined significantly from emission order 3 to 4 and from 6 to 7, increased from 7 to 8, and declined again from 8 to 9. *Methylocella* decreased from 5 to 6 and increased from 6 to 7, whereas *Methylacidiphilum* declined from 2 to 3, increased from 5 to 6, and declined again from 6 to 7.

Figure 3

Functional restructuring of the curated CH_4-cycling community across the CH_4 flux gradient. The heatmap shows z-scored within-genus changes in mean relative abundance for curated methanogenic and methanotrophic genera across CH_4 emission orders (1–9). The leftmost column (“F”) indicates the assigned metabolic pathway of each taxon. Arrows within tiles denote significant ($p \leq 0.05$) stepwise changes between adjacent emission orders based on pairwise t-tests with Benjamini–Hochberg correction; upward arrows indicate increases and downward arrows indicate decreases in within-group relative abundance.

Indicator taxa along the CH_4 gradient

Indicator species analysis identified 17 taxa significantly associated with specific CH_4 emission orders ($p \leq 0.05$; 999 permutations). Most indicator taxa were associated with emission order 2, including a diverse set of methanogenic genera spanning hydrogenotrophic, acetoclastic/mixotrophic, and methylotrophic pathways. The strongest indicators were *Methanothermococcus* (IndVal = 0.405, p = 0.001), *Methanohalobium* (IndVal = 0.393, p = 0.001), *Methanohalophilus* (IndVal = 0.383, p = 0.001), *Methanosaeta* (IndVal = 0.380, p = 0.001), and *Methanocella* (IndVal = 0.379, p = 0.001). Several additional methanogenic taxa, including *Methanopyrus*, *Methanocorpusculum*, *Methanococcoides*, and *Methanothermus*, also showed strong associations with emission order 2.

In contrast, methanotrophic indicators occurred at intermediate positions along the gradient. The Type I methanotroph *Methylococcus* was significantly associated with CH_4 emission order 3 (IndVal = 0.351, p = 0.005), whereas the Type II methanotroph *Methylosinus* was associated with CH_4 emission order 4 (IndVal = 0.351, p = 0.005). These results suggest that lower emitting mesocosms were characterized by a broader suite of methanogenic taxa, whereas methanotrophic indicators emerged at intermediate positions along the flux gradient.

Figure 4. Indicator genera associated with CH_4 emission orders in the CH_4-cycling community. Bars show the group-equalized indicator value (IndVal.g) for microbial genera significantly associated with a given CH_4 emission order ($p \leq 0.05$). Higher IndVal.g values indicate a stronger and more specific association between a genus and that emission-order group. Colors denote the indicator rank shown in the legend. Only significant indicator genera are displayed.

Discussion

This study aimed to determine whether CH_4-cycling microbial communities vary within a single vegetation type and to identify indicator taxa associated with different magnitudes of CH_4 flux. Despite all mesocosms being dominated by *Eriophorum vaginatum*, we observed substantial variation in CH_4 emissions among mesocosms. Similar fine-scale heterogeneity has previously been reported within visually uniform wetland and peatland vegetation units [31, 32]. The coexistence of strong CO_2 uptake and strong CH_4 release is also well documented in sedge dominated wetlands [33–35]. In addition to these ecosystem scale patterns, the microbial dataset showed that both sides of the CH_4 cycle were well represented, with methanotrophs accounting for approximately 55% of the CH_4-cycling community and methanogens 45%. Thus, both CH_4 production and oxidation potential were substantial components of the microbial assemblage. Across the gradient, increasing CH_4 emissions were accompanied by higher Reco but not higher GPP, indicating intensified belowground carbon processing rather than reduced ecosystem productivity.

Although light, air temperature, and water-table depth were held constant, CH_4 emissions varied markedly among mesocosms. Fluxes more than doubled from the lowest- to the highest emitting

mesocosms, indicating substantial heterogeneity within the same plant functional type. Comparable sharp transitions in CH_4 flux have been reported within sedge-dominated peatlands [36, 37], where microscale hydrology or peat chemistry can lead to threshold like responses [38, 39]. In the present experiment, however, hydrological conditions were controlled. We therefore suggest that the steep increase at the upper end of the gradient may reflect threshold behavior in methanogenic activity, where microbial responses accelerate once substrate availability or redox conditions pass critical levels. While our taxonomic data are consistent with this interpretation, confirming the mechanism would require transcript level evidence.

Consistent with our first aim, CH_4-cycling microbial communities differed in composition along the CH_4 flux gradient despite similar vegetation structure, water-table depth, temperature, and light intensity. These differences reflected shifts in the relative abundance of CH_4-cycling functional groups rather than broad taxonomic turnover. Acetoclastic and mixotrophic methanogens, such as *Methanosarcina*, increased in higher-emitting mesocosms, whereas the dominant hydrogenotrophic methanogen *Methanoregula* declined modestly across the gradient. Several additional hydrogenotrophic taxa also showed smaller decreases, suggesting a gradual redistribution of methanogenic pathways rather than wholesale community replacement. Such shifts are consistent with changes in substrate availability and redox microsite conditions and suggest a transition toward more metabolically flexible methanogens. The modest reduction in the otherwise dominant *Methanoregula* further supports the idea that increased CH_4 emissions may reflect a broadening of methanogenic substrate use, potentially linked to enhanced rhizodeposition and fermentation products in productive wet soils.

Similar substrate-driven transitions have been widely reported in peatland and wetland systems [40]. For example, Kotsyurbenko et al. [41] and Popp et al. [42] showed that high substrate and acetate availability can stimulate *Methanosarcina* dominance, coinciding with enhanced CH_4 fluxes. In Finnish fens, Juottonen et al. [43] observed that increases in labile organic substrates following shifts in plant productivity led to replacement of hydrogenotrophic taxa by acetoclastic methanogens. Comparable functional restructuring was reported by McCalley et al. [40] in thawing permafrost peatlands, where elevated acetate concentrations and lower redox potentials shifted methanogenic pathways from hydrogenotrophic to acetoclastic dominance and accelerated CH_4 release. Likewise, Rinne et al. [44] concluded from variation in $\delta^{13}C$ values of emitted CH_4 in a hemi-boreal mire that spatial variability in CH_4 emissions was primarily controlled by differences in methanogenic substrate availability rather than by methanotrophy. Together, these studies support the view that microscale peat chemistry, particularly redox potential and the abundance of fermentative intermediates, can induce threshold-like shifts in methanogenic community composition and activity, leading to pronounced changes in CH_4 flux even under otherwise similar environmental conditions.

Methanotrophs comprised a substantial proportion of the CH_4-cycling community and exhibited compositional shifts along the gradient. The *Verrucomicrobial* methanotroph *Methylacidiphilum* declined substantially in higher-emitting mesocosms, whereas the Type II methanotroph *Methylosinus* increased slightly. Despite the relatively high overall abundance of methanotrophs, changes in individual taxa

suggest that functional CH_4 oxidation potential did not scale proportionally with increasing CH_4 production. Such decoupling between production and oxidation is consistent with physical limitations imposed by oxygen diffusion and the expansion of micro-anoxic zones in saturated soils [45, 46]. Similar findings have been reported in peatlands where methanotroph abundance or activity did not increase with elevated CH_4 availability, indicating that oxidation is often constrained by microscale O_2 gradients rather than substrate supply [38]. Overall, these observations suggest that while increased CH_4 production may stimulate some Type II methanotrophs, CH_4 oxidation potential in water-saturated systems is primarily limited by O_2 diffusion and microsite redox structure rather than by methanotroph abundance alone. More broadly, these findings indicate that microbial functional composition varies within a vegetation-consistent peatland ecotype and that shifts in both methanogenic and methanotrophic guilds contribute to spatial CH_4 flux heterogeneity independently of vegetation identity [47].

Addressing our second aim, indicator species analysis identified taxa associated with distinct positions along the CH_4 flux gradient. Most indicator taxa were associated with CH_4 emission order 2, including a broad suite of methanogenic genera spanning hydrogenotrophic, acetoclastic/mixotrophic, and methylotrophic pathways. The strongest indicators were *Methanothermococcus*, *Methanohalobium*, *Methanohalophilus*, *Methanosaeta*, and *Methanocella*. Several additional methanogenic taxa, including *Methanopyrus*, *Methanocorpusculum*, *Methanococcoides*, and *Methanothermus*, also showed strong associations with emission order 2. In contrast, methanotrophic indicators occurred at intermediate positions along the gradient, with the Type I methanotroph *Methylococcus* associated with emission order 3 and the Type II methanotroph *Methylosinus* with emission order 4. These results suggest that the lower end of the CH_4 gradient was characterized by diverse methanogenic assemblages, whereas methanotrophic taxa became more indicative at intermediate CH_4 emission levels.

Taken together, the results show that CH_4-cycling microbial communities can vary substantially within a single vegetation-defined peatland system. Variation in methanogenic metabolic strategies, together with shifts in methanotrophic community composition, appears to contribute to spatial CH_4 flux heterogeneity that is not captured by vegetation or hydrological models alone. Incorporating microbial functional composition into wetland CH_4 models may therefore improve predictions of CH_4 emission dynamics and associated climate feedback. More broadly, the CH_4 flux gradient reflects not only variation in emission rates but also variation in the underlying microbial ecology, with CH_4-cycling pathways shifting across the gradient in a manner indicative of strongly reduced microsites and accelerated carbon turnover [40, 41].

These findings reinforce the idea that vegetation structure, hydrology and temperature are not sufficient to predict CH_4 cycling alone and suggest that microbial communities, often treated as static or implicitly parameterized in many CH_4 models, may be key drivers of observed flux differences. Current models, including those embedded in larger Earth system frameworks such as LPJ-GUESS [49], often link CH_4 production to coarse large-scale generalizations. Our results instead point to the value of more microbially explicit modelling approaches, such as CLM-Microbe [51] and JULES-microbe [14], that can

better resolve small-scale variation within a single plant functional type. Dynamic models that respond to feedback among redox conditions, substrate pools, and microbial community structure may offer a path forward for better capturing observed CH_4 variability.

At the same time, the practical implementation of microbial and redox feedback in predictive models remains constrained by data availability, parameter uncertainty, and scale mismatch. Redox potential, substrate pool dynamics, and microbial community structure are highly heterogeneous at the microscale, whereas most land-surface and Earth system models operate at spatial resolutions of tens of kilometers. Capturing such fine scale feedback would require explicit representation of microsite hydrology, pore connectivity, and dynamic oxygen diffusion, which are rarely measured and remain difficult to parameterize [16, 14]. Moreover, comparisons between microbial-explicit models and simpler empirical or process-based approaches often show only modest improvements in predictive skill [52, 53]. Until measurement techniques and data-assimilation frameworks improve, simpler semi-empirical models that parameterize CH_4 dynamics through environmental proxies may remain more robust at ecosystem or regional scales.

Conclusion

This study shows that substantial CH_4 flux variability can emerge within a single vegetation-defined peatland ecotype and that this variability is associated with compositional shifts in the underlying CH_4-cycling microbial community. Despite consistent hydrological and physical conditions, mesocosms dominated by *Eriophorum vaginatum* exhibited more than twofold variation in CH_4 emissions, corresponding to distinct microbial assemblages across the CH_4 cycle.

Low-emission mesocosm orders were characterized by taxa associated with relatively constrained methanogenic conditions, such as *Methanosaeta* and *Methanocella*, whereas higher emitting mesocosm orders showed increased representation of metabolically flexible taxa such as *Methanosarcina*. Methanotrophs comprised a substantial fraction of the CH_4-cycling community and shifted compositionally along the gradient, with taxa such as *Methylococcus* and *Methylosinus* associated with intermediate positions along the CH_4 gradient. However, methanotrophic restructuring did not scale proportionally with increasing CH_4 production, suggesting that oxidation in these saturated soils may be constrained primarily by microsite oxygen availability rather than CH_4 supply [45, 46].

Collectively, these findings highlight that microscale functional diversity and redox-dependent microbial strategies, rather than vegetation type alone, contribute to spatial CH_4 flux variation in peatlands. Models that assume homogeneous microbial processes may therefore underestimate within ecosystem heterogeneity. By demonstrating a clear linkage between microbial functional composition and CH_4 flux magnitude, this work provides an empirical framework for integrating microbial ecology into process-based CH_4 models and advancing predictive understanding of wetland carbon climate feedback.

Methods

Site description

We collected nine peat-plant mesocosms from Fäjemyr, an ombrotrophic bog in Skåne, southern Sweden (56°15'53.3"N, 13°33'14.1"E). The peatland is classified as an eccentric bog and is characterized by semi-forested areas alternating between raised hummocks, hollows, and moss lawns [22, 23]. Long-term (1961–1990) mean annual temperature and precipitation are 6.2°C and 700 mm, respectively [24]. Peat depth ranges between 4 and 5 m, and peat water pH is generally below 4 throughout the growing season [23].

Vegetation composition at Fäjemyr is diverse, including hummocks dominated by dwarf shrubs such as *Calluna vulgaris* and *Erica tetralix*. Moss lawns are carpeted with Sphagnum species, including *S. magellanicum* and *S. rubellum*, whereas the drier hummocks support dwarf Scots pine (*Pinus sylvestris*). The dominant sedge species at the site is *Eriophorum vaginatum* [22, 23].

Experimental design

A total of nine cylindrical mesocosms (height 26 cm, diameter 27 cm) were collected on 30 March 2017. Mesocosms were assigned arbitrary identifiers (1–9) at collection, carefully cut from the peatland, and transferred directly into plastic containers for transport to Lund University (82 km away), where they were incubated in a temperature- and light-controlled growth room.

During the first month, air temperature was set to 10°C under dark conditions. Temperature and light levels were then gradually increased to allow the mesocosms to acclimate and to simulate the onset of the growing season. During the final four weeks of the experiment, conditions in the growth room were maintained at 20°C and 500 µmol PAR m^{-2} s^{-1}, with 17 h of daylight based on sunrise and sunset at Fäjemyr. Because of heat radiation from the lamps, temperature varied diurnally from 18 ± 0.3°C when lamps were off to 23 ± 1°C when lamps were on. Light intensity also varied somewhat across the table surface owing to differences in individual lamp efficiency (512 ± 42 µmol PAR m^{-2} s^{-1}). To minimize spatial bias in growth conditions, mesocosms were rotated bi-weekly among positions on the table.

All mesocosms were watered daily with deionized water to maintain a constant water-table depth at the surface. During the final three weeks of the experiment, CH_4 fluxes were measured bi-weekly (n = 6 measurements per mesocosm). At the end of the experiment, individual peat samples were removed from three positions in each mesocosm: the upper oxic–anoxic interface (5 cm), deeper peat (15 cm), and root-adjacent peat (rhizosphere). This yielded a total of 27 peat samples for genomic analysis (3 samples per mesocosm).

Flux measurements

CH_4 and CO_2 fluxes were measured using the static chamber method [12, 25]. For each mesocosm, 6-minute measurements were performed using a transparent 5 L cylindrical polycarbonate chamber equipped with a rubber seal to ensure airtight closure and a fan to circulate air. CH_4 and CO_2 concentrations were measured at 1 Hz with an LGR Fast Greenhouse Gas Analyzer (model 911 – 0010,

Los Gatos Research, CA, USA). Fluxes were calculated from the change in gas concentration over time using linear fitting and were corrected for air pressure, chamber volume, and chamber temperature. Positive flux values indicate emission, whereas negative values indicate uptake.

Captured metagenomics

Peat samples and DNA extraction

Peat material was collected from three positions within each mesocosm: the upper oxic–anoxic interface (5 cm), deeper peat (15 cm), and root-adjacent peat directly attached to the root surface (10 cm). Samples were stored at − 20°C and thawed at 4°C before DNA extraction. DNA was extracted using the DNeasy® PowerSoil® Kit (Qiagen, Hilden, Germany) according to the manufacturer's protocol with 0.25 g input material. DNA quality (A260/A280) and concentration were assessed using a NanoDrop Lite (NanoDrop Technologies, Wilmington, NC, USA) and a Qubit 4 fluorometer (Thermo Fisher Scientific, Waltham, MA, USA), respectively.

SeqCap EZ probe generation, library generation, and sequencing

Metagenomic DNA extracted from peat was processed to enrich target sequences using the captured metagenomics method established by White et al. [21] for peatland environments. Genes encoding enzymes related to CH_4 production and consumption were identified from the Kyoto Encyclopaedia of Genes and Genomes (KEGG) database [26] and compiled into a local CH_4 database (Supplementary Table 1). The nucleotide coding sequences in this database were used to design custom hybridization-based probes for sequence capture according to Kushwaha et al. [27], suitable for the NimbleGen SeqCap EZ protocol (Roche NimbleGen Inc., Madison, USA).

Pre-capture libraries were prepared according to the NimbleGen SeqCap EZ HyperCap Workflow User's Guide (Version 1.0, June 2016), with two modifications to improve hybridization efficiency: (i) 5 µL of 15 µM KAPA unique dual-index mixed adapters were used during adapter ligation instead of single-index adapters, and (ii) pre-capture PCR used seven cycles for libraries prepared from 150 ng genomic DNA and five cycles for libraries prepared from 1 µg genomic DNA.

Libraries were multiplexed in pools of 15 in equimolar amounts and fragment sizes, with 1 µg of each pool transferred to a tube and hybridized to the custom probes according to the NimbleGen SeqCap EZ SR User's Guide (Version 4.3, October 2014). Final captured libraries were sequenced on an Illumina HiSeq4000 platform to generate 2 × 150 bp paired-end reads. Sequencing was carried out by the Centre for Genomic Research, University of Liverpool, United Kingdom.

Data analysis

Raw FASTQ files were trimmed for Illumina adapter sequences using Cutadapt v1.2.1 [28]. Low-quality bases were removed with Sickle v1.200 using a sliding-window Phred threshold of 20 and reads shorter

than 20 bp after trimming were discarded [29]. Processed reads from each captured dataset were uploaded to MG-RAST for annotation [30]. Default MG-RAST quality filters were applied (maximum e-value 1e − 5, minimum alignment length 15 bp, minimum identity 60%) to remove low-quality and duplicate sequences. Functional and taxonomic annotations were then filtered to the methane metabolism pathway, KEGG ko:00680. Taxonomy was assigned against RefSeq [31] within MG-RAST and exported to R for downstream analysis (details in Supplementary Methods).

Statistical analysis

Carbon fluxes across the CH_4 gradient

All analyses were conducted in R and visualized with ggplot2 [32]. Mean CH_4 flux was calculated for each mesocosm and inspected using histograms, Q–Q plots, and Shapiro–Wilk tests. Mesocosms retained their original identifiers, but for analysis they were additionally ordered from lowest to highest mean CH_4 flux and assigned a CH_4 emission order from 1 (lowest mean flux) to 9 (highest mean flux). This ordinal variable was used to represent position along the observed CH_4 flux gradient.

For mixed-effects analyses using emission order, CH_4 and Ecosystem Respiration (R_{eco}) were transformed using log1p, whereas Gross Primary Production (GPP) and Net Ecosystem Exchange (NEE) were transformed using the inverse hyperbolic sine transformation. Normality of transformed variables was assessed after transformation using Shapiro–Wilk tests and visual inspection of histograms. Linear mixed-effects models were fit with CH_4 emission order as a fixed effect and replicate as a random intercept to account for repeated measurements, using the lme4 package [33]. Model significance was tested using likelihood-ratio tests comparing the full model with a random-effects-only model, and post hoc pairwise comparisons among emission orders were obtained from estimated marginal means with Tukey adjustment [34].

To examine associations between CH_4 and CO_2 flux components, separate ordinary least squares regressions were fit for CH_4 versus R_{eco}, CH_4 versus GPP, and CH_4 versus NEE using the base R lm() function. We report adjusted R^2 and two-sided p-values for slopes. For visualization, quadratic smoothers with 95% confidence bands were overlaid, although inference is based on the fitted linear term.

Flux–tillers relationships (mixed-effects regression)

To test whether plant productivity predicted gas fluxes, CH_4, GPP, R_{eco}, and NEE were each modelled as a function of tiller density (Tillers). Response variables were transformed using the inverse hyperbolic sine transformation, and linear mixed-effects models were fit with scaled tiller density as a fixed effect and CH_4 emission order as a random intercept. This transformation behaves similarly to a logarithmic transform for large values, improving linearity and variance stabilization, but, unlike the log transform, it is defined at zero and for negative fluxes. This allowed us to model the full distribution of greenhouse-gas fluxes without discarding zero-flux measurements or artificially shifting the data.

Models were fit with lmer() in the lme4 package [33]. Fixed-effect p-values for Tillers were obtained via Satterthwaite t-tests when lmerTest was available; otherwise, likelihood-ratio tests were used to compare full and reduced models. Variance explained by fixed effects was summarized as marginal R^2 using the performance package [28], and model predictions with 95% confidence intervals were generated using ggeffects and back-transformed for plotting. Model assumptions were checked using residual-versus-fitted and Q–Q plots.

Community heatmap and consecutive-order tests

Each genus was assigned to a CH_4-cycling guild representing their primary metabolic pathway (i.e. hydrogenotrophic methanogenesis; acetoclastic and mixotrophic methanogenesis; methylotrophic methanogenesis; Type I methanotrophy; Type II methanotrophy; Verrucomicrobial methanotrophy; and low-abundance/unclassified). Within each sample, abundances were normalized separately within methanogen and methanotroph groups to obtain within-group relative composition. Mean relative composition was then calculated for each genus across CH_4 emission orders and standardized within genus using z-scores. Thus, the heatmap color scale reflects relative change along the flux gradient rather than baseline abundance.

Pairwise t-tests were performed for genus-level within-group relative composition across emission orders, after which only consecutive contrasts (1–2, 2–3, …, 8–9) were retained. P-values were adjusted using the Benjamini–Hochberg false discovery rate correction, and significant increases or decreases were denoted with directional arrows based on changes in mean relative abundance between adjacent emission orders. Genera were ordered by metabolic pathway and overall mean relative abundance to aid interpretation. The final visualization combined a functional sidebar (guild color key) with a diverging z-score heatmap centered at 0.

Indicator species analysis

To identify microbial taxa associated with distinct positions along the CH_4 flux gradient, we performed indicator species analysis using the multipatt function in the indicspecies R package [35]. This method evaluates the strength and significance of associations between taxa and predefined groups, here the CH_4 emission orders 1–9, by considering both occurrence frequency and exclusivity across groups.

Analyses were conducted on Hellinger-transformed genus abundance data, using CH_4 emission order as the grouping variable. Statistical significance was assessed using 999 permutations, and taxa with $p \leq 0.05$ were considered significant indicators of one or more positions along the CH_4 gradient.

Declarations

Acknowledgements

We would like to thank Pia and the staff from the Centre for Genomic Research, Ulrika from Roche Diagnostics Scandinavia, colleagues, friends and family for the valuable discussions and Oskar Ström

for laboratory assistance. The data handling was enabled by resources in project (SNIC 2019/8-365) provided by the Swedish National Infrastructure for Computing (SNIC) at UPPMAX, partially funded by the Swedish Research Council through grant agreement no. 2018-05973.

Author contributions

Conceptualization: J.D.W., L.S., F.-J.W.P
Methodology: J.D.W., L.S., D.A., J.R.
Investigation: J.D.W.
Formal analysis: J.D.W., F.-J.W.P, L.S.
Data curation: J.D.W., V.L.
Validation: J.D.W., D.A., V.L.
Resources: L.S.
Supervision: L.S., F.-J.W.P
Funding acquisition: L.S., D.A.
Writing – original draft: J.D.W., L.S., F.-J.W.P
Writing – review & editing: J.D.W., D.A., F.-J.W.P., V.L., J.R., L.S.
Visualization: J.D.W.

Data availability statement

The annotated metagenomes are available at the MG-RAST server under the project ID: 91052. In addition, all raw sequences will be made public via NCBI Bio Project ID: PRJNA691743 upon acceptance of this manuscript. Processed datasets, including methane (CH_4) flux measurements and microbial community composition data, are available in the Zenodo repository at https://doi.org/10.5281/zenodo.19234000. All other data and scripts supporting the findings of this study are available from the corresponding author upon reasonable request.

Additional Information

The authors declare that they have no conflict of interest. In addition, the authors declare that they have no known financial or non-financial competing interests that could have appeared to influence the work reported in this paper.

Funding Declaration

J.D.W., D.A., F-J.W.P, V.L, J.R. and L.S. discloses support for the research underlying this work from Vetenskapsrådet (VR: **2018-05973)**, The Swedish Research Council for Sustainable Development (FORMAS: 997-610) and The Crafoord Institute (20200783).

References

1. Dean, J. F. et al. Methane Feedbacks to the Global Climate System in a Warmer World. *Rev. Geophys.* **56** (1), 207–250 (2018).
2. Dlugokencky, E. J. et al. Atmospheric methane levels off: Temporary pause or a new steady-state? Geophysical Research Letters, 30(19). (2003).
3. Saunois, M. et al. Global Methane Budget 2000–2020. *Earth Syst. Sci. Data Discuss.*, : 1–147. (2024).
4. Ferry, J. G. Fundamentals of methanogenic pathways that are key to the biomethanation of complex biomass. *Curr. Opin. Biotechnol.* **22** (3), 351–357 (2011).
5. Finlayson, C. M., Milton, G. R., Peatlands & *in The Wetland Book: II: Distribution, Description, and Conservation* Dordrecht. 227–244 (Springer Netherlands, 2018).
6. Hakobyan, A. & Liesack, W. Unexpected metabolic versatility among type II methanotrophs in the Alphaproteobacteria. *Biol. Chem.* **401** (12), 1469–1477 (2020).
7. Hanson, R. S. & Hanson, T. E. Methanotrophic bacteria. *Microbiol. Rev.* **60** (2), 439–471 (1996).
8. Hao, Y. et al. Soil moisture controls over carbon sequestration and greenhouse gas emissions: a review. *npj Clim. Atmospheric Sci.* **8** (1), 16 (2025).
9. Mastepanov, M. et al. Revisiting factors controlling methane emissions from high-Arctic tundra. *Biogeosciences* **10** (7), 5139–5158 (2013).
10. Ström, L., Mastepanov, M. & Christensen, T. R. Species-specific Effects of Vascular Plants on Carbon Turnover and Methane Emissions from Wetlands. *Biogeochemistry* **75** (1), 65–82 (2005).
11. Ström, L. et al. Presence of Eriophorum scheuchzeri enhances substrate availability and methane emission in an Arctic wetland. *Soil Biol. Biochem.* **45**, 61–70 (2012).
12. Crill, P. M. et al. Methane flux from Minnesota Peatlands. *Glob. Biogeochem. Cycles*. **2** (4), 371–384 (1988).
13. Sun, L. et al. Temporal and spatial variability of methane emissions in a northern temperate marsh. *Atmos. Environ.* **81**, 356–363 (2013).
14. Chadburn, S. E. et al. Modeled Microbial Dynamics Explain the Apparent Temperature Sensitivity of Wetland Methane Emissions. Global Biogeochemical Cycles, 34(11): e2020GB006678. (2020).
15. Wania, R., Ross, I. & Prentice, I. C. Implementation and evaluation of a new methane model within a dynamic global vegetation model: LPJ-WHyMe v1.3.1. *Geosci. Model Dev.* **3** (2), 565–584 (2010).
16. Bridgham, S. D. et al. Methane emissions from wetlands: biogeochemical, microbial, and modeling perspectives from local to global scales. *Glob. Change Biol.* **19** (5), 1325–1346 (2013).
17. Fierer, N., Barberán, A. & Laughlin, D. C. Seeing the forest for the genes: using metagenomics to infer the aggregated traits of microbial communities. *Front. Microbiol.* **5**, 614 (2014).
18. Galand, P. E., Fritze, H. & Yrjala, K. Microsite-dependent changes in methanogenic populations in a boreal oligotrophic fen. *Environ. Microbiol.* **5** (11), 1133–1143 (2003).

19. Gasc, C., Peyretaillade, E. & Peyret, P. Sequence capture by hybridization to explore modern and ancient genomic diversity in model and nonmodel organisms. *Nucleic Acids Res.* **44** (10), 4504–4518 (2016).
20. Manoharan, L. et al. Captured metagenomics: large-scale targeting of genes based on sequence capture reveals functional diversity in soils. *DNA Res.* **22** (6), 451–460 (2015).
21. White, J. D. et al. Methane Producing and Oxidizing Microorganisms Display a High Resilience to Drought in a Swedish Hemi-Boreal Mire. Journal of Geophysical Research: Biogeosciences, 128(9): e2022JG007362. (2023).
22. Lonnstad, J. & Löfroth, M. *Myrskyddsplan för Sverige* (Stockholm, Sweden, 1994).
23. Lund, M. et al. Annual CO_2 balance of a temperate bog. *Tellus B*. **59** (5), 804–811 (2007).
24. SMHI, Klimat i förändring. En jämförelse av temperatur och nederbörd 1991–2005 med 1961–1990. Swedish Meteorological and Hydrological Institute: Norrköping, Sweden. (2006).
25. Livingston, G. & Hutchinson, G. Enclosure-based measurement of trace gas exchange: applications and sources of error. In: Biogenic Trace Gases: Measuring Emissions from Soil and Water, 51: 14–51. (1995).
26. Kanehisa, M. et al. KEGG as a reference resource for gene and protein annotation. *Nucleic Acids Res.* **44** (D1), D457–D462 (2015).
27. Kushwaha, S. K. et al. MetCap: a bioinformatics probe design pipeline for large-scale targeted metagenomics. *BMC Bioinform.* **16**, 65 (2015).
28. Nakagawa, S., Johnson, P. C. D. & Schielzeth, H. The coefficient of determination R^2 and intra-class correlation coefficient from generalized linear mixed-effects models revisited and expanded. *J. Royal Soc. Interface*. **14** (134), 20170213 (2017).
29. Benjamini, Y. & Hochberg, Y. Controlling the False Discovery Rate: A Practical and Powerful Approach to Multiple Testing. *J. Roy. Stat. Soc. B*. **57** (1), 289–300 (1995).
30. Kassambara, A. rstatix: Pipe-Friendly Framework for Basic Statistical Tests. R package version 0.7.2, (2023).
31. Korrensalo, A. et al. Small spatial variability in methane emission measured from a wet patterned boreal bog. *Biogeosciences* **15** (6), 1749–1761 (2018).
32. Ström, L. et al. Controls of spatial and temporal variability in CH_4 flux in a high arctic fen over three years. *Biogeochemistry* **125** (1), 21–35 (2015).
33. Christensen, T. R. et al. Biotic controls on CO_2 and CH_4 exchange in wetlands – a closed environment study. *Biogeochemistry* **64** (3), 337–354 (2003).
34. Bellisario, L. M. et al. Controls on CH_4 emissions from a northern peatland. *Glob. Biogeochem. Cycles*. **13** (1), 81–91 (1999).
35. Wu, J. et al. Simulation of six years of carbon fluxes for a sedge-dominated oligotrophic minerogenic peatland in Northern Sweden using the McGill Wetland Model (MWM). *J. Geophys. Research: Biogeosciences*. **118** (2), 795–807 (2013).

36. Riutta, T. et al. Interacting effects of vegetation components and water level on methane dynamics in a boreal fen. *Biogeosciences* **17** (3), 727–740 (2020).
37. Stewart, G. A. et al. High spatial variability in wetland methane fluxes is tied to vegetation patch types. *Biogeochemistry* **167** (12), 1589–1607 (2024).
38. Perryman, C. R. et al. Microtopography Matters: Belowground CH_4 Cycling Regulated by Differing Microbial Processes in Peatland Hummocks and Lawns. Journal of Geophysical Research: Biogeosciences, 127(8): e2022JG006948. (2022).
39. Boonman, J. et al. Redox potential is a robust indicator for decomposition processes in drained agricultural peat soils: A valuable tool in monitoring peatland wetting efforts. *Geoderma* **441**, 116728 (2024).
40. McCalley, C. K. et al. Methane dynamics regulated by microbial community response to permafrost thaw. *Nature* **514** (7523), 478–481 (2014).
41. Kotsyurbenko, O. R. et al. Competition between homoacetogenic bacteria and methanogenic archaea for hydrogen at low temperature. *FEMS Microbiol. Ecol.* **38** (2–3), 153–159 (2001).
42. Popp, T. J. et al. Evaluation of methane oxidation in the rhizosphere of a Carex-dominated fen in north-central Alberta, Canada. *Biogeochemistry* **51** (3), 259–281 (2000).
43. Juottonen, H. et al. Seasonality of rDNA- and rRNA-derived archaeal communities and methanogenic potential in a boreal mire. *ISME J.* **2** (11), 1157–1168 (2008).
44. Rinne, J. et al. Spatial and temporal variation in δ13C values of methane emitted from a hemiboreal mire: methanogenesis, methanotrophy, and hysteresis. *Biogeosciences* **19** (17), 4331–4349 (2022).
45. Rey-Sanchez, C. et al. The ratio of methanogens to methanotrophs and water-level dynamics drive methane transfer velocity in a temperate kettle-hole peat bog. *Biogeosciences* **16** (16), 3207–3231 (2019).
46. Zhang, H. et al. Methane production and oxidation potentials along a fen–bog gradient from southern boreal to subarctic peatlands in Finland. *Glob. Change Biol.* **27** (18), 4449–4464 (2021).
47. Arnold, W. et al. Microbial activity contributes to spatial heterogeneity of wetland methane fluxes. *Microbiol. Spectr.*, **11**(5). (2023).
48. Bräuer, S. L. et al. Methanogenic archaea in peatlands. *FEMS Microbiol. Lett.*, **367**(20). (2020).
49. Smith, B., Prentice, I. C. & Sykes, M. T. Representation of vegetation dynamics in the modelling of terrestrial ecosystems: comparing two contrasting approaches within European climate space. *Glob. Ecol. Biogeogr.* **10** (6), 621–637 (2001).
50. Wania, R. et al. Present state of global wetland extent and wetland methane modelling: methodology of a model inter-comparison project (WETCHIMP). *Geosci. Model Dev.* **6** (3), 617–641 (2013).
51. He, L. et al. Dynamics of Fungal and Bacterial Biomass Carbon in Natural Ecosystems: Site-Level Applications of the CLM-Microbe Model. Journal of Advances in Modeling Earth Systems, 13(2): e2020MS002283. (2021).

52. Meng, L. et al. Sensitivity of wetland methane emissions to model assumptions: application and model testing against site observations. *Biogeosciences* **9** (7), 2793–2819 (2012).
53. Xu, X. et al. Reviews and syntheses: Four decades of modeling methane cycling in terrestrial ecosystems. *Biogeosciences* **13** (12), 3735–3755 (2016).

Figures

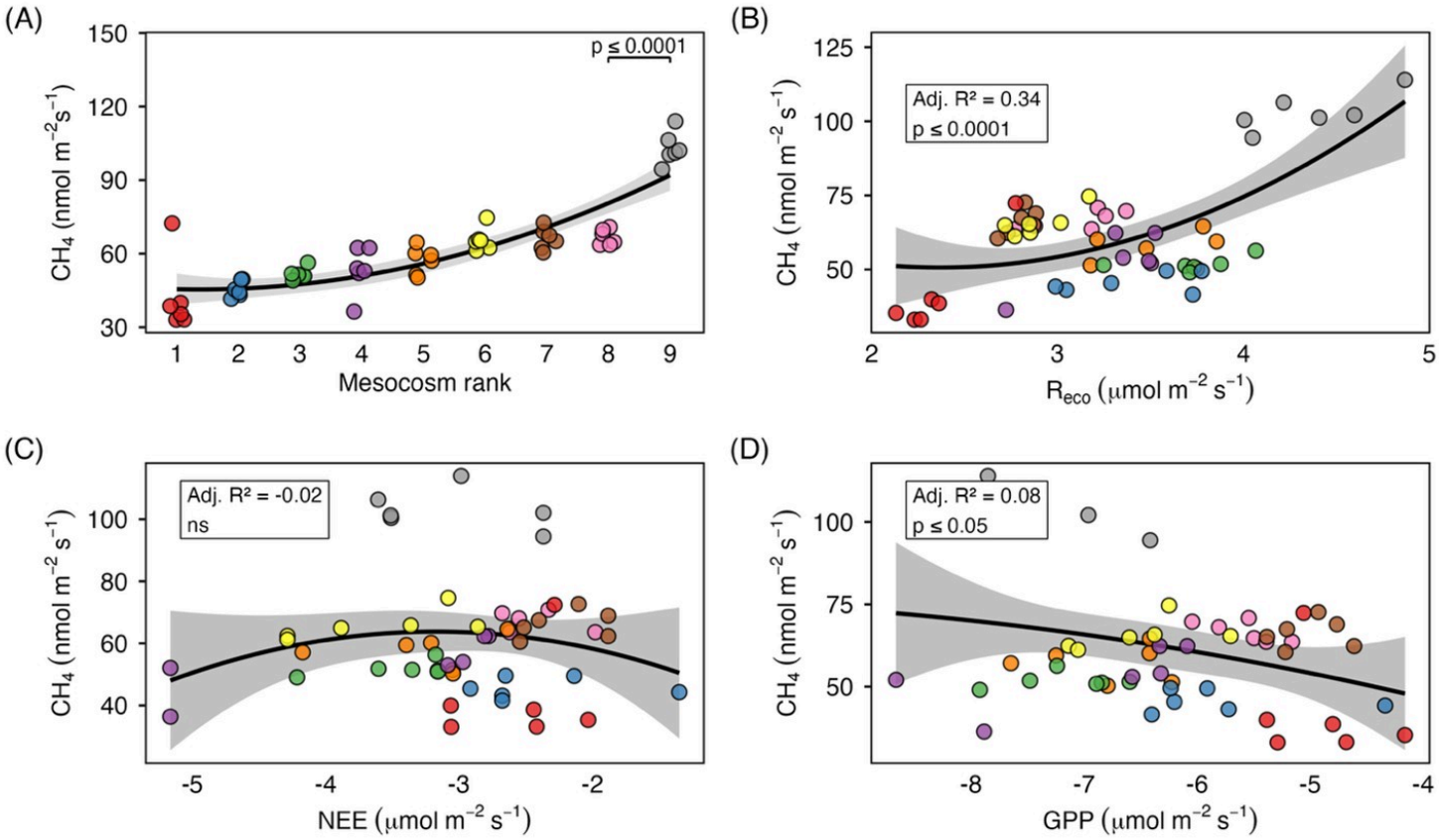

Figure 1

CH_4 fluxes across all emission orders (1–9) (A), and linear regressions between CH_4 flux and (B) ecosystem respiration (R_{eco}), (C) net ecosystem exchange (NEE), and (D) gross primary productivity (GPP). Points represent individual flux measurements (n = 54). Solid lines represent fitted polynomial regressions and shaded areas indicate ±95% confidence intervals. Adjusted R^2 and p-values from linear models are shown in panels B–D.

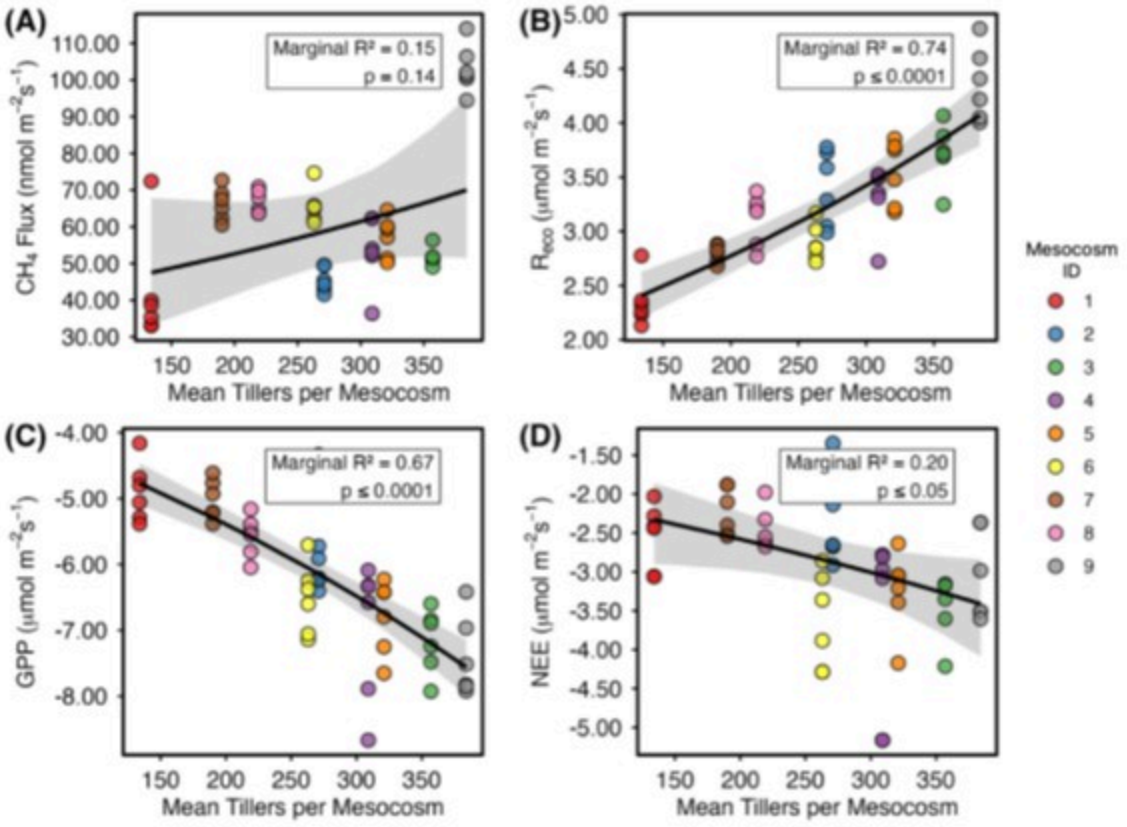

Figure 2

Carbon fluxes of (A) methane (CH_4), (B) ecosystem respiration (Reco), (C) net ecosystem exchange (NEE), and (D) gross primary productivity (GPP) plotted against mean tiller density per mesocosm. Points represent individual mesocosms coloured by CH_4 emission order. Fitted lines and shaded ribbons show model predictions and 95% confidence intervals derived from linear mixed-effects models. Reported statistics indicate marginal R^2 and p-values for the effect of tiller density on each flux.

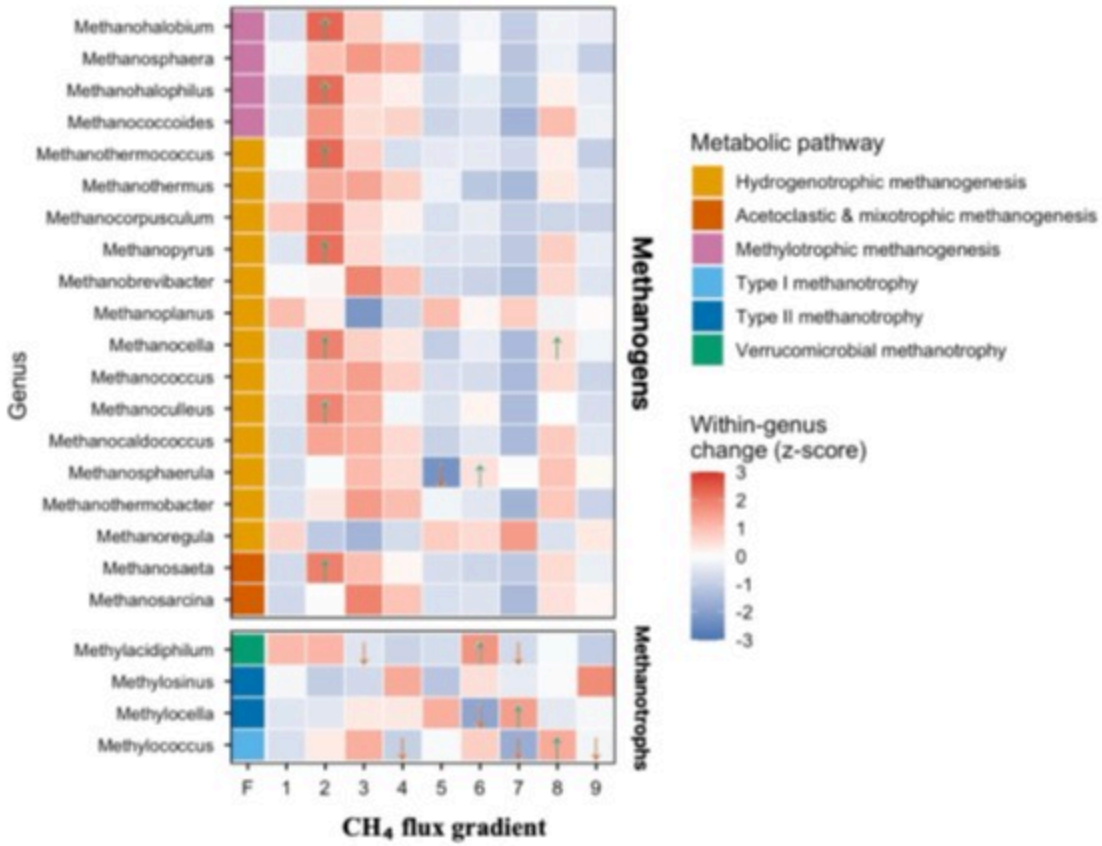

Figure 3

Functional restructuring of the CH_4-cycling community across the CH_4 flux gradient. The heatmap shows z-scored within-genus changes in mean relative abundance for curated methanogenic and methanotrophic genera across CH_4 emission orders (1–9). The leftmost column (“F”) indicates the assigned metabolic pathway of each taxon. Arrows within tiles denote significant ($p \leq 0.05$) stepwise changes between adjacent emission orders based on pairwise t-tests with Benjamini–Hochberg correction; upward arrows indicate increases and downward arrows indicate decreases in within-group relative abundance.

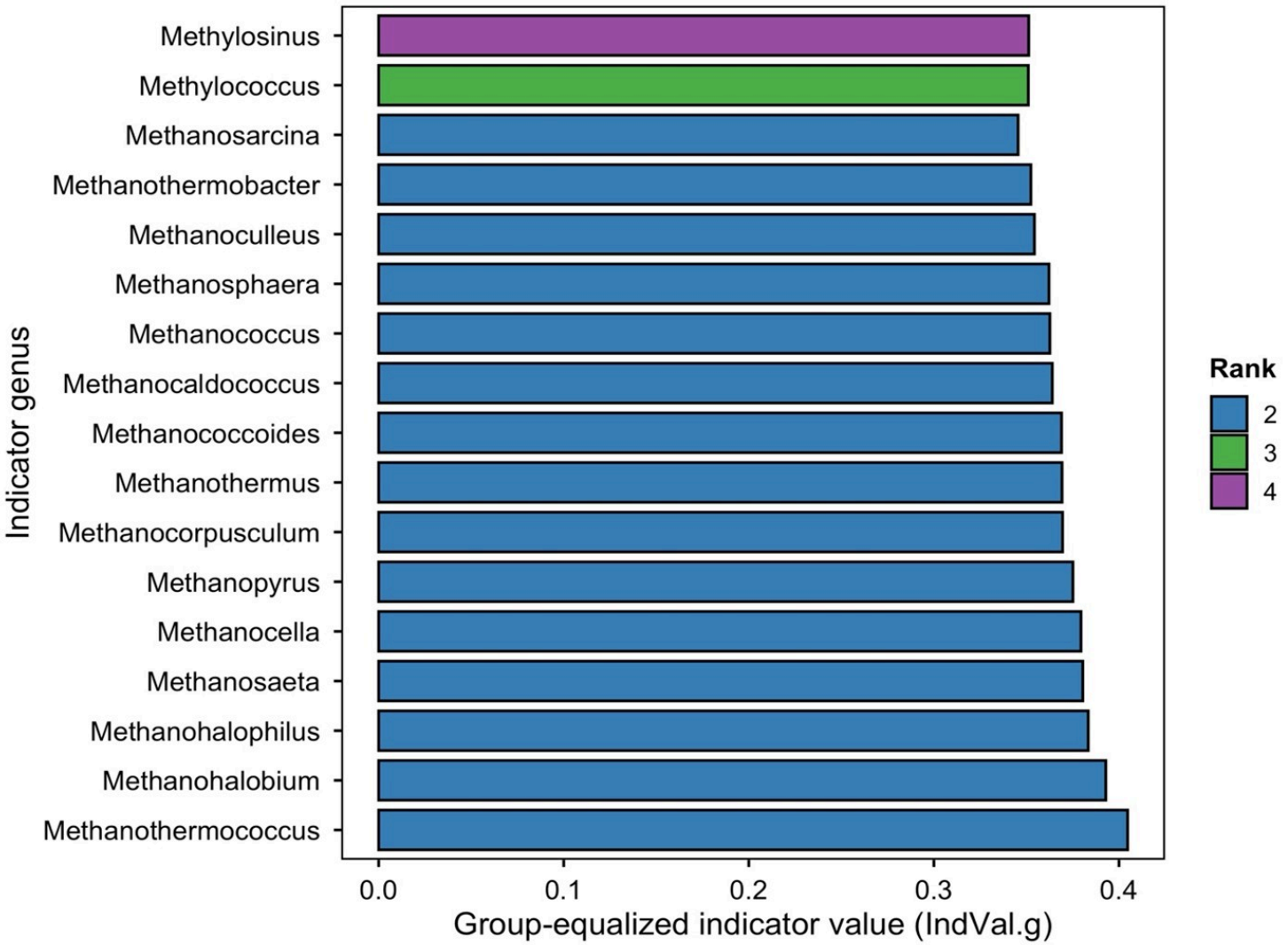

Figure 4

Indicator genera associated with CH_4 emission orders in the CH_4-cycling community. Bars show the group-equalized indicator value (IndVal.g) for microbial genera significantly associated with a given CH_4 emission order ($p \leq 0.05$). Higher IndVal.g values indicate a stronger and more specific association between a genus and that emission-order group. Colors denote the indicator rank shown in the legend. Only significant indicator genera are displayed.